Journal of Drug Delivery Science and Technology 111 (2025) 107155

Contents lists available at ScienceDirect

Journal of Drug Delivery Science and Technology

journal homepage: www.elsevier.com/locate/jddst

SILAC-based nuclear proteomics uncovers antitumor mechanisms of selenium nanoparticles with in vivo validation in a melanoma model

Hector Estevez [a], Estefania Garcia-Calvo [a], Roberto Álvarez-Fernández Garcia [a], Raquel Sanchez-Diaz [b,c], Juan José Lazcano [b], Pilar Martin [b,c], Jose L. Luque-Garcia [a,*]

[a] Department of Analytical Chemistry, Faculty of Chemical Sciences. Complutense University of Madrid, 28040, Madrid, Spain
[b] Centro Nacional de Investigaciones Cardiovasculares (CNIC), Madrid, Spain
[c] Centro de Investigación em Red de Enfermedades Cardiovasculares (CIBER-CV), 28029, Madrid, Spain

ARTICLE INFO

Keywords:
Ch-SeNPs
SILAC
Cancer treatment
Quantitative proteomics
Cell cycle arrest
Nanomedicine
In-vivo assessment

ABSTRACT

Chitosan-stabilized selenium nanoparticles (Ch-SeNPs) are promising agents for cancer therapy due to their unique physicochemical properties, including spherical morphology and uniform size distribution. This study investigates the molecular mechanisms underlying their antitumoral effects, with a focus on the nuclear proteome. Quantitative proteomic analysis revealed 343 nuclear proteins, 47 of which showed significant changes following Ch-SeNPs treatment. Key regulators such as CDK1 and CDC5 were implicated in cell cycle arrest and tumor suppression pathways. Ch-SeNPs also affected processes including mRNA metabolism and cytoskeleton organization. In addition, Ch-SeNPs significantly inhibited tumor growth in a murine melanoma model, supporting their therapeutic potential.

1. Introduction

In the current field of cancer treatments, nanotechnology has emerged as a crucial player [1], offering innovative approaches to combat tumors with enhanced precision and efficacy [2,3]. Nanoparticles enable targeted drug delivery [4], minimizing side effects, and enhancing therapeutic efficacy [5]. Their ability to cross biological barriers and specifically target cancer cells holds great promise in providing novel oncological interventions [6,7].

Among the different types of nanoparticles that are currently being under study for tumor treatments, selenium nanoparticles (SeNPs) are particularly interesting, since they have already shown their ability to induce cell cycle arrest and senescence, thus impairing tumoral growth [8,9]. However, although some of the biomolecular mechanisms by which SeNPs exert their action have already been studied, there is still a need for a better understanding of such pathways, specially at the nuclear level where these SeNPs seems to play a particularly relevant role.

Proteomics, particularly quantitative proteomics, is a suitable technique for unraveling the mechanisms of action of novel antitumor agents [10]. By identifying and quantifying protein changes, quantitative proteomics approaches offer a comprehensive understanding of the molecular processes underlying the effects of new antitumor compounds [11]. Among the different strategies, stable isotopic labeling by amino acids in cell culture (SILAC) remains the most widely employed strategy, due to its high accuracy and versatility [12]. The method involves growing two populations of cells: one in a culture medium containing normal ("light") amino acids and the other in a medium with isotopically labeled ("heavy") amino acids. Over time, the cells incorporate these amino acids into their proteins, resulting in one population with "light" proteins and another with "heavy" proteins. After the incorporation period, the two cell populations are combined, and their proteins are extracted, digested into peptides, and analyzed using mass spectrometry. The mass spectrometer can distinguish between the "light" and "heavy" peptides based on their mass differences. By comparing the signal intensities of the corresponding "light" and "heavy" peptides, the relative abundance of proteins between the two cell populations can be determined [13].

Analyzing the entire cellular proteome presents significant challenges due to its complexity, dynamic range, and the vast number of proteins involved, which can hinder the detection of subtle but functionally important alterations [14]. Focusing on specific subcellular compartments, such as the nucleus, helps reduce this complexity and increases analytical sensitivity and selectivity. The rationale for targeting the nuclear proteome lies in the nucleus central role in regulating

* Corresponding author.
E-mail address: jlluque@ucm.es (J.L. Luque-Garcia).

https://doi.org/10.1016/j.jddst.2025.107155
Received 21 January 2025; Received in revised form 4 June 2025; Accepted 5 June 2025
Available online 6 June 2025

gene expression, DNA replication, and cell cycle progression, which are processes frequently disrupted in cancer. In addition, Ch-SeNPs have been shown to affect these nuclear functions, particularly transcriptional regulation and cell cycle control [15]. Therefore, nuclear proteomics may allow for the identification of targets and pathways that might remain undetected in whole-cell lysates.

Based on the above, in this work we have used the SILAC strategy in combination with a nuclear protein purification method to gain insights into the mechanisms of action of Ch-SeNPs at the nuclear level. Furthermore, in addition to finding important targets responsible for the cytotoxic action of this NPs in tumor cells, an in vivo experiment using a murine model of melanoma has been carried out, which has allowed us to evaluate the efficacy of Ch-SeNPs treatment in a more complex environment. The results obtained have contrasted previous studies and have supported the therapeutic potential of Ch-SeNPs as an antitumor agent.

2. Materials and methods

2.1. Synthesis and characterization of Ch-SeNPs

Chitosan-stabilized selenium nanoparticles (Ch-SeNPs) were synthesized following a previously published procedure [16]. Briefly, 7.5 mL of 0.23 M ascorbic acid and 5 mL of 2.4 M acetic acid were mixed with 10 mL of an aqueous chitosan polysaccharide solution (0.5 % w/v). Afterwards, 0.51 M sodium selenite was slowly added to the mixture. The formation of Ch-SeNPs were noted through the change of the dispersion from colorless to red. Then, 10 mL of the dispersion were dialyzed against 2 L of distilled water using a 12 kDa MWCO membrane for 2 h at room temperature. Synthesized Ch-SeNPs were stored at 4 °C up to two months.

Synthesized Ch-SeNPs were observed by Transmission Electron Microscopy (TEM). Droplets of the dispersion were placed onto a holey carbon film on copper grids. Micrographs were obtained with a JEOL JEM 1400 PLUS operating at 120 kV.

2.2. Cell culture

Two cell types were employed in this work: HepG2, used in the in vitro experiments, and B16 cells, used in the in vivo experiments. HepG2 cells were maintained in Dulbecco's modified Eagle's medium (DMEM) supplemented with 10 % fetal bovine serum (FBS) and 1 % penicillin/streptomycin at 37 °C and 5 % CO_2. B16 cells were cultured in DMEM, supplemented with 10 % FBS, L-glutamine and penicillin and streptomycin at 37 °C in a humidified 5 % CO_2 atmosphere. Cells were harvested under exponential growth, centrifuged and placed in $1x10^6$/50 μl of PBS before injection.

2.3. Quantitative proteomics

2.3.1. Metabolic labeling

HepG2 cells were maintained in DMEM supplemented with 10 % dialyzed FBS, 100 units per 100 mL of penicillin/streptomycin and either naturally occurring isotopes ("light") or stable isotope-labeled ("heavy") $^{13}C_6$ arginine and lysine amino acids. Culture media were refreshed when 80% (8×10^6 cells) plate confluence was reached and the cells were grown for at least 6 doublings to allow full incorporation of the labeled amino acids. To verify the complete incorporation of $^{13}C_6$-Lys and $^{13}C_6$-Arg in isotopically heavy medium after eight cell divisions, an MS analysis of a protein digest was performed (data not shown). The SILAC-based quantitative proteomics analysis was conducted using two independent biological replicates.

2.3.2. Exposure to Ch-SeNPs and isolation of nuclear proteins

HepG2 cells labeled with "heavy" (direct SILAC) or "light" (reverse SILAC) amino acids were exposed to 1 mg/L of Ch-SeNPs for 72 h. The concentration of Ch-SeNPs and the exposure time were selected based on previous studies [15], as these conditions have been shown to induce an approximately 50 % reduction in cell viability, providing a suitable model for evaluating cellular responses to treatment. Cells grown in either "light" or "heavy" media were harvested, counted and mixed in a 1:1 ratio. Then, isolation of nuclear proteins was carried out with the Qproteome Nuclear Protein kit (Qiagen). Briefly, cells were washed with PBS and centrifuged 5 min at 450×*g* (4 °C). Once cells were resuspended in 500 μL of lysis buffer, 25 μL of detergent solution were added and vortex mixed for 10 s. Cells were centrifuged 5 min at 10,000×*g* (4 °C). Afterwards, the pellet (which contains cell nuclei) was re-suspended in nuclear protein lysis buffer. After 5 min centrifugation at 10,000×*g*, the nuclear pellet was re-suspended in 50 μL of extraction buffer NX1. The mixture was then incubated for 30 min at 4 °C and centrifuged at 12000×*g* for 10 min. The nucleic-acid binding proteins were isolated in the supernatant. For the extraction of "insoluble" nuclear proteins, the pellet was re-suspended in 100 μL of extraction buffer NX2 and incubated for 1 h. Finally, the suspension was centrifuged at 12,000×*g* for 10 min to obtain the "insoluble" nuclear proteins fraction.

2.3.3. SDS-page and in-gel digestion

Proteins were separated by means of SDS-PAGE on 10 % SDS-polyacrylamide gels. After electrophoresis and Coomassie Brilliant Blue staining, gel lanes were cut into approximately 20 sections. Gel bands were de-stained in 25 mM ammonium bicarbonate/50 % acetonitrile, cut into smaller pieces, dehydrated with acetonitrile and dried. Gel pieces were incubated with a 12.5 ng/μL trypsin solution in 25 mM ammonium bicarbonate overnight at 37 °C. To extract the peptides, gel pieces were incubated with acetonitrile and 5 % formic acid, dried using vacuum centrifugation and reconstituted in 12 μL of and aqueous solution containing 2 % acetonitrile and 0.1 % formic acid.

2.3.4. Mass spectrometry analysis

Analysis was performed with a nanoflow LC-MS/MS. Peptides fractions were loaded onto a C18 trap column (0.3 × 10 mm, SGE) and then separated on a reverse-phase column (75 μm × 25 cm fused silica capillary C18 HPLC PepMap column, 3 μm, 100 A, Thermo) selecting a linear gradient of 5–95 % acetonitrile in 0.1 % aqueous solution of formic acid. A nano LC ultra 1D plus system (Eksigent) delivered the mentioned gradient at a flow-rate of 200 nL/min through the analytical column up to a stainless nano-bore emitter (Proxeon). An LTQ XL linear ion trap mass spectrometer (Thermo Scientific) scanned and fragmented the peptides operating in data-dependent Zoom Scan and MS/MS switching mode using the three most intensive precursor ions detected in a survey scan from 400 to 1600 u (three scans). In order to monitor the entire $^{12}C/^{13}C$ isotopic envelope of most doubly and triply charged peptides, the ZoomScan mass window was set to 12 Da. Singly charged ions were excluded for MS/MS analysis. Resulting raw files were converted to mgf files to enable MASCOT database search. The Uniprot Homo sapiens data base was searched using the MASCOT protein identification software (v2.3 MatrixScience). Search restrictions were set: trypsin specificity with one missed cleavage allowed, methionine oxidation and $^{13}C_6$-Arg and $^{12}C_6$-Lys as variable modifications. Minimum precursor and fragment-ion mass accuracies for 1.2 and 0.3 Da were used. At least one unique peptide (bold-red peptides meaning highest scoring peptide matching to protein with highest total score) was required for protein identification and at least two unique peptides were required for quantification. The cut-off values for MASCOT scores of peptides and proteins were set to 40 ($p < 0.05$) and 46 ($p < 0.01$), respectively. The false positive rate was estimated by searching the same spectra against the Uniprot Homo Sapiens decoy database. QuiXoT open-source software (version 1.3.26) was used to calculate the relative quantification ratios (R_{SILAC}) of identified proteins based on peak area. Verification of all protein ratios obtained by QuiXoT was carried out by manually inspecting all quantified peptides.

2.4. Gene expression analysis

Trizol reagent (Invitrogen) was employed to isolate total RNA from HepG2 cells exposed to Ch-SeNPs (1 mg/L and 72 h). The quantity of extracted RNA was measured using a NanoDrop One (Thermo Fisher Scientific). A Quantitec reverse transcription kit (Qiagen) was used for the synthesis of cDNAs and for the integrated removal of genomic DNA contamination. For the RT-qPCR analysis, TaqMan gene expression assays and TaqMan Fast advance master mix (Thermo Fischer Scientific) were used according to manufacturer's instructions. The references of Taqman gene expression assays used are listed in Table 1. The relative expression of genes was normalized using GAPDH as the endogenous control. Gene expression in each sample was calculated as 2–ΔΔCt. All RT-qPCR analyses were carried out using the same biological replicates employed in the SILAC proteomics experiments to ensure consistency across datasets.

2.5. In-vivo inhibition of melanoma tumor growth

12 weeks old females in the C57BL/6J background, weighting ~20–25 g, were injected intradermally (ID) in both sides of the back with $1x10^6$ B16 cells. Animals were housed and used in specific pathogen-free (SPF) conditions at the CNIC (Spanish National Center for Cardiovascular Research) animal facility. All animal procedures were approved by the ethics committee of the Comunidad Autónoma de Madrid and conducted in accordance with the institutional guidelines that comply with the European Institutes of Health's; Directive 2010/63/EU of the European Parliament and the Council on the Protection of Animals Used for Scientific Purposes (Official Journal of the European Union. Vol. 53:33–79, 2010). 5 days after intradermal B16 injections, tumors became established (~50 mm3) into the mice at the minimum size to begin the treatment with the NPs. A control group of non-treated mice was analyzed in parallel. Ch-SeNPs were prepared at a final concentration of 200 mg/L 50 μl of vehicle (synthesis media) alone or containing Ch-SeNPs were injected intra tumor with a 25G needle in the right and left back sides, respectively. Treatment as described was performed on alternate days. The mice body weights and tumor sizes were recorded on alternate days after treatment. The tumor size was determined by Ratio (Ref. 6369H15) digital caliper measurements and calculated as length x width x height. After 10–15 days, mice with tumors >1.5 cm in diameter were sacrificed. The tumor suppression rate (TSR) was calculated to quantify the antitumor efficacy of Ch-SeNPs treatment compared to control and vehicle groups. For each animal, tumor volume was measured at each timepoint of the experiment using digital calipers. The TSR for day 13 was calculated according to the following formula:

$$TSR(\%) = [1 - \text{Mean tumor volume of treated group}/\text{Mean tumor volume of control group}] \times 100$$

The mean tumor volume for each group was determined by averaging the tumor volumes of all animals in that group at the end of the treatment period. TSR values were calculated for the Ch-SeNPs-treated group in comparison to both the control group and the vehicle-treated group. The resulting percentage represents the degree of tumor growth inhibition induced by the treatment relative to the reference group.

Table 1
References of TaqMan gene expression assays used for the RT-PCR analysis.

Gene	RefSeq	Assay ID
CDK1	NM_001170406	Hs00938777_m1
CCNB1	NM_031966.3	Hs01030099_m1
CCNA2	NM_001237.3	Hs00996788_m1
CDKN1A	NM_000389.4	Hs00355782_m1
GAPDH	NM_001256799.2	Hs03929097_g1

3. Results and discussion

3.1. Characterization of Ch-SeNPs

Although the synthesis of Ch-SeNPs has been previously carried out with an extensive physico-chemical characterization, TEM micrographs were acquired in order to verify the size and morphology of the newly synthesized Ch-SeNPs. As shown in Fig. 1, well-dispersed Ch-SeNPs were obtained, with nanoparticles exhibiting spherical morphology and homogeneous sizes of around 40–60 nm.

3.2. Mechanisms of action of Ch-SeNPs at the nuclear level

In previous studies [8,9], we identified some of the biomolecular mechanisms of action related to the antitumoral potential of Ch-SeNPs. Since some of these findings were directly related with the action of Ch-SeNPs over nuclear proteins, we designed a SILAC-based assay focused on the nuclear proteome, in order to gain deeper insights into these mechanisms. Thus, we conducted an extensive SILAC experiment (Fig. 2) that included purification of the nuclear proteome. 343 proteins were identified, with 236 meeting the criteria for protein quantitation. These criteria include the identification of at least two unique peptides with a MASCOT score >46 ($p < 0.01$). The majority of these proteins exhibited a SILAC ratio close to 1, as expected for a 1:1 mixture. Applying a threshold ratio of 1.30, commonly used in quantitative proteomics to define biologically relevant changes, we identified 47 altered proteins, with 22 upregulated and 25 downregulated upon Ch-SeNPs exposure (Table 2).

A false discovery rate of 0.3 % was estimated by the number of hits against the reverse sequence/total hits ($p < 0.01$). The mean relative standard deviation (RSD) of ratios obtained from biological replicates was lower than 20 %, indicating good agreement between experiments. Subcellular localization of each protein was checked in Gene Ontonlogy (GO) database and confirmed that more than 62 % of identified proteins came from the nucleus, 31 % from cytoplasm, 3 % from endoplasmic reticulum, 2 % from mitochondria and 2 % from plasma membrane, thus showing the usefulness of the purification protocol followed to enrich nuclear proteins. We also categorized the proteins based on their molecular and cellular functions using GO database, and the results pointed out that exposure to Ch-SeNPs mainly affected the mRNA metabolism, the cell cycle and the transcription process.

The antitumor potential of Ch-SeNPs, demonstrated in previous studies [15,59], involves the arrest of the cell cycle in the S-G2/M phase. The protein CDK1 ($R_{SILAC} = -1.46$), known for promoting replicative DNA synthesis, was identified as the primary factor responsible for the G2/M phase cell cycle arrest [17]. Our quantitative proteomics findings further support this cell cycle arrest by confirming the inhibition of CDK1 and other affected proteins. Since no other crucial proteins directly involved in the cell cycle were detected, we conducted gene expression analysis using the qPCR technique (Fig. 3). This experiment validated the inhibition of CDK1 and revealed alterations in other genes that corroborate the cell cycle arrest. P21 upregulation (CDKN1A), known to inhibit the kinase activity of CDK1 [18], along with the inhibition of CCNB1 and CCNA1, which form a complex with CDK1 and are essential for cell progression into mitosis [19,20] were among the confirmed effects.

Among the proteins experiencing deregulation, CDC5 ($R_{SILAC} = -1.39$) stands out as a vital component of the pre-mRNA splicing complex, crucial for cell cycle progression in yeast, plants, and mammals (Fig. 4). There is evidence suggesting CDC5L overexpression in various tumors, including glioma and hepatocellular carcinoma. Knockdown of CDC5L has been shown to significantly impede tumor cell proliferation in glioma and hepatocellular carcinoma by inducing cell cycle arrest at the G2/M phase. In osteosarcoma, CDC5L overexpression has been linked to poor prognosis, making its inhibition a potential therapeutic strategy [21,22]. Other deregulated proteins play key roles in sister

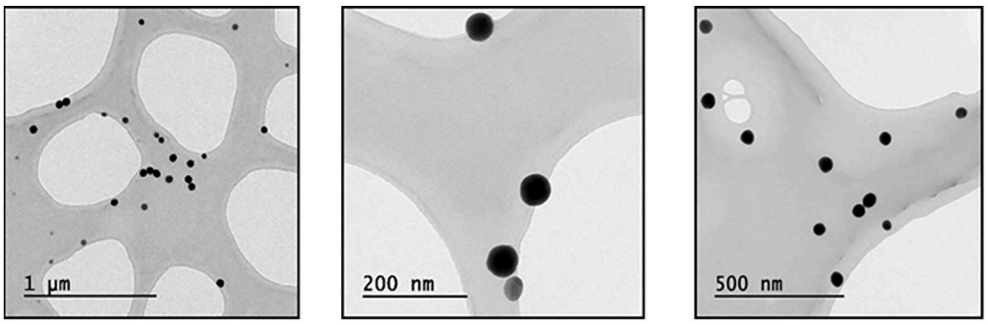

Fig. 1. TEM micrographs show the synthesized Ch-SeNPs exhibiting a spherical morphology and homogeneous sizes ranging from 40 to 60 nm.

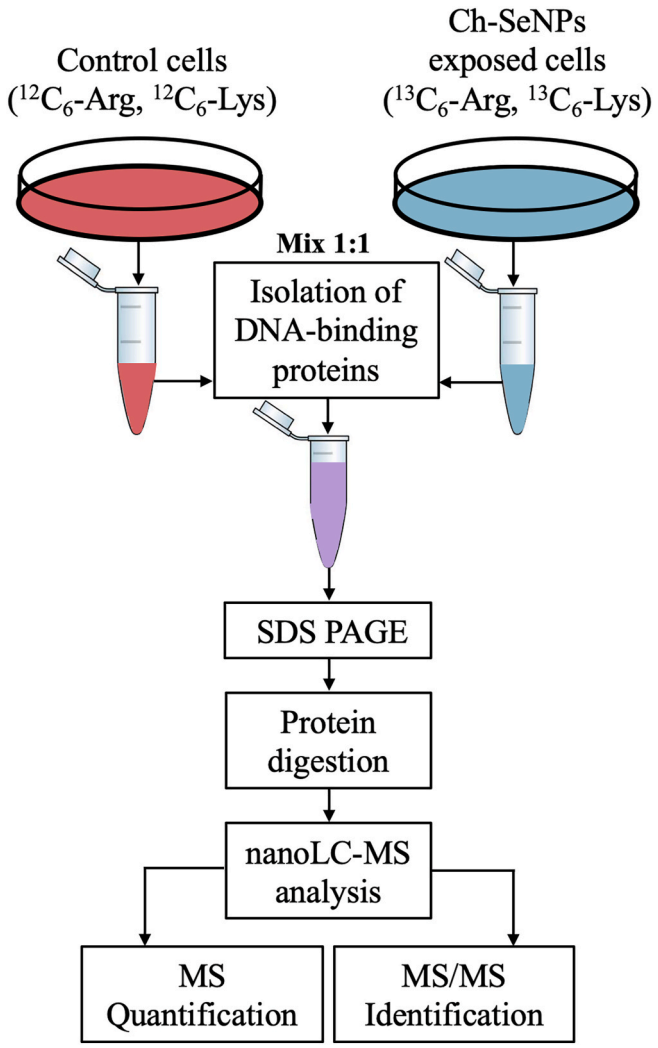

Fig. 2. Schematic representation of the SILAC-based quantitative proteomics approach used to identify key nuclear proteins involved in the antitumor effect of Ch-SeNPs.

chromatids cohesion and condensation during the mitosis process, essential for proper chromosome segregation from the S phase to metaphase. SMC1 (R_{SILAC} = −1.45) is instrumental in establishing linkages between duplicated DNAs during the S phase, contributing to DNA damage repair and maintaining genomic stability. Inhibiting SMC1 has been associated with growth suppression in various cancer cells through G1/S cell cycle phase arrest [23–25]. WAPL (R_{SILAC} = −1.37) and its interaction with PDS5B (R_{SILAC} = −1.33), both inhibited by Ch-SeNPs, are crucial in the cohesion process. Human WAPL expression has been linked to tumor progression, and inhibiting this protein arrests cells at the S phase [26]. Another protein required for chromosome segregation during mitosis is ERH (R_{SILAC} = −1.30), essential for recovering from cell cycle arrest induced by compounds like Ch-SeNPs. RNAi-mediated ERH knockdown leads to G2/M arrest [27–29]. Related to cell cycle arrest, CHC1 (R_{SILAC} = −1.41) and AP2B1 (R_{SILAC} = −1.44), both downregulated by Ch-SeNPs, play roles in membrane trafficking and mitosis. Altered CHC function could contribute to oncogenesis, as CHC inhibition results in growth arrest, cessation of DNA synthesis, overduplication of centrosomes, and senescence [30–33]. On a different note, NOLC1 (R_{SILAC} = 1.92), a phosphoprotein essential for rRNA synthesis and ribosome biosynthesis, induces a DNA damage response at telomeres when overexpressed, promoting apoptosis and cell cycle arrest [34,35].

Certain deregulated proteins, despite not having a direct association with the cell cycle, exemplify the notable ability of Ch-SeNPs to significantly diminish tumors, making their expression modifications a subject of clinical interest (Fig. 4). PLEC (R_{SILAC} = −4.07), for instance, while it plays a critical role in organizing the cytoskeleton network in normal cells, its expression and mislocalization in tumor cells contribute to tumor progression. Silencing PLEC expression in pancreatic cancer cells has been demonstrated to negatively impact proliferation, invasion, and migration [36]. Another intriguing protein is SUMO2 (R_{SILAC} = −1.78), involved in reversible post-translational modification known as sumoylation. This modification is crucial for maintaining genomic integrity, regulating gene expression, and intracellular signaling. Numerous studies have established SUMO-regulated mechanisms in various cancers, and the inhibition of this protein has shown promise in reducing tumors. Consequently, compounds inhibiting SUMO are undergoing clinical trials for cancer treatment [37,38]. RSU1 (R_{SILAC} = −1.40), an oncoprotein influencing cellular proliferation, differentiation, survival, and gene expression, has been associated with cancer development. Approximately 30 % of human tumors harbor RSU1 mutations, with certain cancers, such as pancreatic cancer, exhibiting RSU1 mutations in nearly 100 % of cases. Similar to SUMO, RSU1 inhibition constitutes a primary objective in numerous anticancer therapies [39–41]. A parallel situation is observed with SMARCC1 (R_{SILAC} = −1.34), a complex contributing to gene expression regulation by altering chromatin structure and enhancing the androgen receptor's transactivation. This protein is upregulated in prostate cancer, and its mutations are present in 20 % of all human cancers [42,43]. Additionally, H1.4 (R_{SILAC} = −1.41), participating in nucleosome spacing and higher-order chromatin structure formation, specifically induces cell proliferation arrest upon depletion [44]. Lastly, PHB (R_{SILAC} = 2.02) regulates mitochondrial respiration activity, and its overexpression represses AR-induced gene activation and suppresses tumor growth, particularly in the context of aging [45].

On another hand, Ch-SeNPs trigger mechanisms that safeguard the cell (Fig. 4). Notably, the protein PRDX1 (R_{SILAC} = 1.38) plays a key role in this group. As an antioxidant protein, PRDX1 mitigates the adverse

Table 2
Differentially expressed proteins in HepG2 cells exposed to 1 mg/L of Ch-SeNPs.

Accession number (gi)	Protein Name	Common Name	R_{SILAC}	RSD (%)
41322923	plectin isoform 1a	PLEC	−4,07	13,81
4506687	40S ribosomal protein S15	RPS15	−2,71	0,86
5453740	myosin regulatory light chain 12A	MYLA12	−1,82	14,59
54792069	small ubiquitin-related modifier 2 isoform a precursor	SUMO2	−1,78	0,89
4504257	histone H2B type 1-C/E/F/G/I	H2BC4	−1,74	19,97
7330335	chloride intracellular channel protein 4	CLIC4	−1,58	18,46
4502709	cyclin-dependent kinase 1 isoform 1	CDK1	−1,46	7,28
30581135	structural maintenance of chromosomes protein 1A	SMC1A	−1,45	12,10
4504445	heterogeneous nuclear ribonucleoprotein A1 isoform a	HNRNPA1	−1,45	16,43
15431288	60S ribosomal protein L10a	RPL10a	−1,44	19,40
4557469	AP-2 complex subunit beta isoform b	AP2B1	−1,44	17,89
4885379	histone H1.4	H14	−1,41	16,00
4758012	clathrin heavy chain 1	CHC1	−1,41	12,69
4758302	enhancer of rudimentary homolog	ERH	−1,40	13,45
4506753	ruvB-like 1	RUVB1	−1,40	3,85
6912638	ras suppressor protein 1 isoform 1	RSU1	−1,40	3,75
11067747	cell division cycle 5-like protein	CDC5	−1,39	9,69
5902076	serine/arginine-rich splicing factor 1 isoform 1	SRSF10	−1,37	14,14
42734325	wings apart-like protein homolog	WAPL	−1,37	14,99
4506697	40S ribosomal protein S20 isoform 2	RPS20	−1,36	11,27
110611218	ribosome-binding protein 1	RBP1	−1,34	14,83
188536047	SWI/SNF complex subunit SMARCC1	SMARCC1	−1,34	7,42
7657269	sister chromatid cohesion protein PDS5 homolog B	PDS5B	−1,33	15,08
21361114	mitochondrial 2-oxogluta-rate/malate carrier protein	M2OM	−1,32	4,83
51477708	heterogeneous nuclear ribonucleoprotein D0 isoform d	HNRNPD	−1,31	2,54
21464101	14-3-3 protein gamma	YWHAG	1,31	2,49
4503477	elongation factor 1-beta	EFB1	1,32	3,98
5031653	pre-mRNA-splicing factor SPF27	SPF27	1,32	5,30
7706326	pre-mRNA branch site protein p14	SF3B6	1,33	16,12
24234747	interleukin enhancer-binding factor 2 isoform 1	ILF3	1,36	20,00
4505591	peroxiredoxin-1	PRDX1	1,38	18,46
47271443	serine/arginine-rich splicing factor 2	SRSF2	1,38	0,17
5031875	lamin isoform C	LMNC	1,38	19,27
62414289	vimentin	VIM	1,39	17,73
304555581	elongation factor 1-delta isoform 1	EFD1	1,41	13,73
11024700	mitochondrial import inner membrane translocase subunit	TIMM13	1,42	7,95
4503249	protein DEK isoform 1	DEK	1,48	17,58
31543164	THO complex subunit 6 homolog isoform 1	THOC5	1,57	19,66
4503507	eukaryotic translation initiation factor 2 subunit 3	EIF2I	1,69	3,81
5803165	protein transport protein Sec61 subunit beta	SEC61B	1,72	19,92
11545813	UPF0428 protein CXorf56 isoform 1	CXorf56	1,79	14,14
148596949	nucleolar and coiled-body phosphoprotein 1	NOLC1	1,92	8,70
4505087	protein mago nashi homolog	MAGOH	1,95	19,75
4505773	prohibitin	PHB	2,02	13,66
7657381	pre-mRNA-processing factor 19	PRPF19	2,03	9,58
16507237	78 kDa glucose-regulated protein precursor	HSPA5	3,57	19,56
12025678	alpha-actinin-4	ACTN4	9,58	3,30

effects of reactive oxygen species (ROS) and exhibits the potential to enhance natural killer cell cytotoxicity while suppressing oncogenic proteins such as c-Myc [46]. Furthermore, there is evidence of activated translation and transcription, reflected in the upregulation of numerous proteins involved in these processes, including SPF27 ($R_{SILAC} = 1.32$), SF3B6 ($R_{SILAC} = 1.33$), ILF3 ($R_{SILAC} = 1.36$), EFB1 ($R_{SILAC} = 1.32$), EFD1 ($R_{SILAC} = 1.41$), THOC5 ($R_{SILAC} = 1.57$), and EIF2I ($R_{SILAC} = 1.69$) [47–50].

Despite these protective responses, certain proteins showed increased expression associated with tumor progression. A notable example is YWHAG ($R_{SILAC} = 1.31$), a protein that plays a crucial role in coordinating cell cycle progression, regulating responses to DNA damage, and is upregulated in melanoma cells resistant to cisplatin, etoposide, fotemustine, or vindesine [51,52]. Another protein showing increased expression is VIM ($R_{SILAC} = 1.39$), whose overexpression impedes apoptosis and enhances invasion [53]. Lastly, DEK ($R_{SILAC} = 1.48$), HSPA5 ($R_{SILAC} = 3.57$), and ACTN4 ($R_{SILAC} = 9.58$) are upregulated proteins whose depletion results in slower tumor growth, making them potential biomarkers associated with malignant phenotypes [53–57].

3.3. *In-vivo inhibition of melanoma tumor growth after Ch-SeNPs exposure*

To study the potential of Ch-SeNPs to suppress tumor growth, we challenge the mice ID with poorly immunogenic tumor cells of melanoma origin in syngeneic C57BL/6J mice. The B16 cell line is widely used as a mouse model for melanoma induction that mimics human melanoma [58]. This subcutaneous model allows the development of ~1 × 1 cm tumors in approximately two weeks, becoming necrotic when they exceed this size. B16–induced melanoma aggressively progresses within a dynamic microenvironment, allowing the study of anti-tumor effect of several molecules. The mice were then ID injected with $1x10^6$ B16 cells in both flanks on day 0 of the experiment. After the formation of a ~50 mm^3, mice were treated intra-tumour (i.t.) with the vehicle alone or with Ch-SeNPs (200 mg/L) in the right and left flank, respectively, on alternate days. The treatment least until the control tumors reach >1.5 cm in diameter, approximately 2 weeks. After treatment, the mice were sacrificed, and the tumors volume calculated (Fig. 5A).

The average volume of the tumor growth was monitored every two days (Fig. 5B). At the beginning of the treatment, on day 5, the average tumor volume of the control mice was 65.234 ± 20.998 mm^3, likely the average volume of the vehicle-treated tumor and the Ch-SeNPs treated tumors was 58.576 ± 21.932 mm^3 and 92.206 ± 25.126 mm^3, respectively, in the same period (Fig. 5B). After 13 days, the average tumor volume of the control increased to 609.078 ± 189.431 mm^3 (8.6-fold increase), the vehicle treated tumors volumen increased to 574.420 ± 127.301 mm^3 (13.2-fold increase) whereas the Ch-SeNPs treated tumors volume barely increased to 119.170 ± 26.604 mm^3, meaning only 1.8-fold increase of the tumor volume in the same period (Fig. 5C). The tumor suppression rate analysis shows significant differences among vehicle mice and Ch-SeNPs treated mice (Fig. 5C).Therefore, i.t.

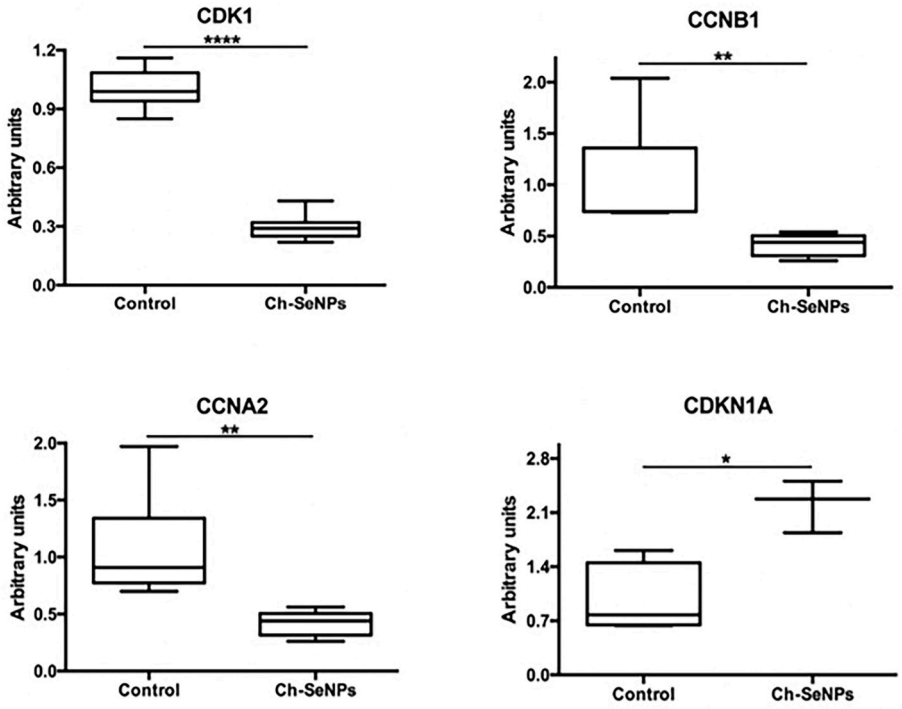

Fig. 3. RT-qPCR-based relative expression analysis of cell cycle-related genes.

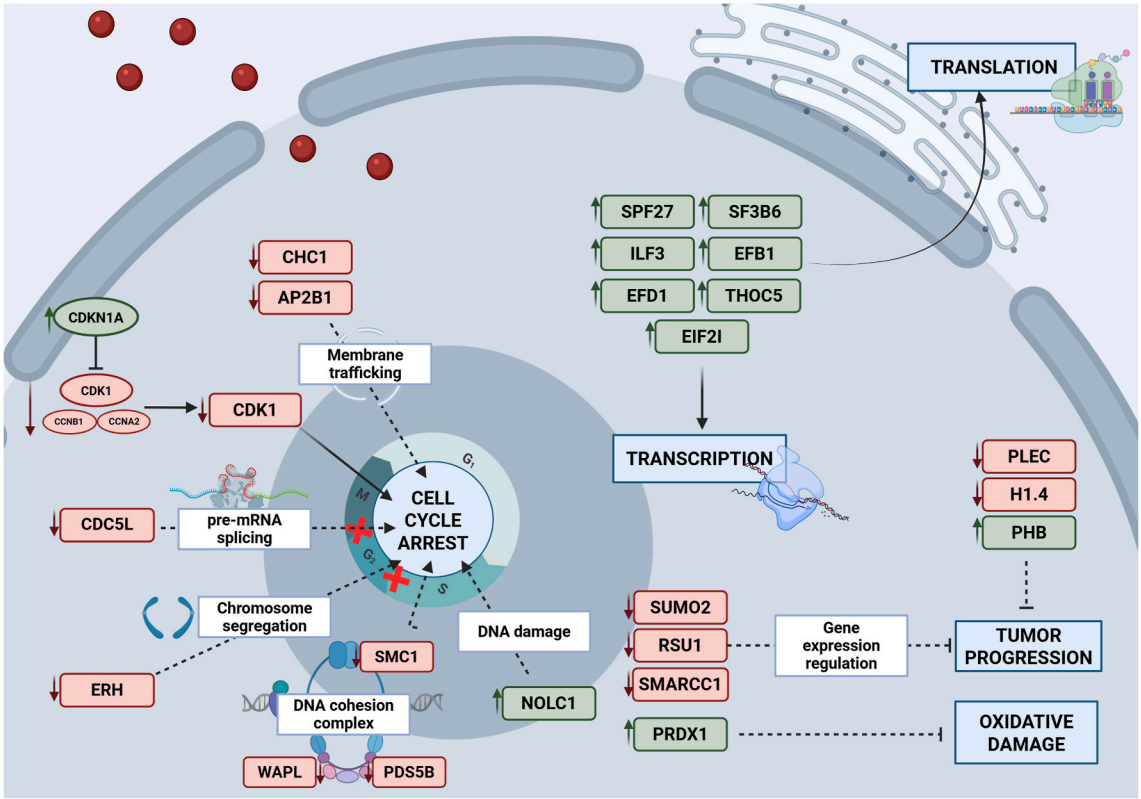

Fig. 4. Schematic diagram illustrating the main cellular pathways implicated in the therapeutic response of Ch-SeNPs. Protein names are shown in rectangles and gene names in circles. Green indicates upregulated biomolecules, while red denotes downregulated ones. Biomolecules are grouped according to the biochemical processes in which they are involved. Ch-SeNPs exert their antitumor effect primarily by inducing cell cycle arrest at the S-G2/M phases through inhibition of CDK1 and its cyclin partners CCNB1 and CCNA1, reinforced by CDKN1A upregulation. Proteomic and transcriptomic analysis confirmed these changes, along with the downregulation of CDC5L, SMC1, WAPL, ERH, CHC1 and other cell division regulators affecting also chromosome cohesion and DNA repair and contributing to cell cycle disruption and genomic instability. Some proteins involved in translation, transcription and oxidative stress response were upregulated, indicating compensatory cell survival mechanisms. (For interpretation of the references to color in this figure legend, the reader is referred to the Web version of this article.)

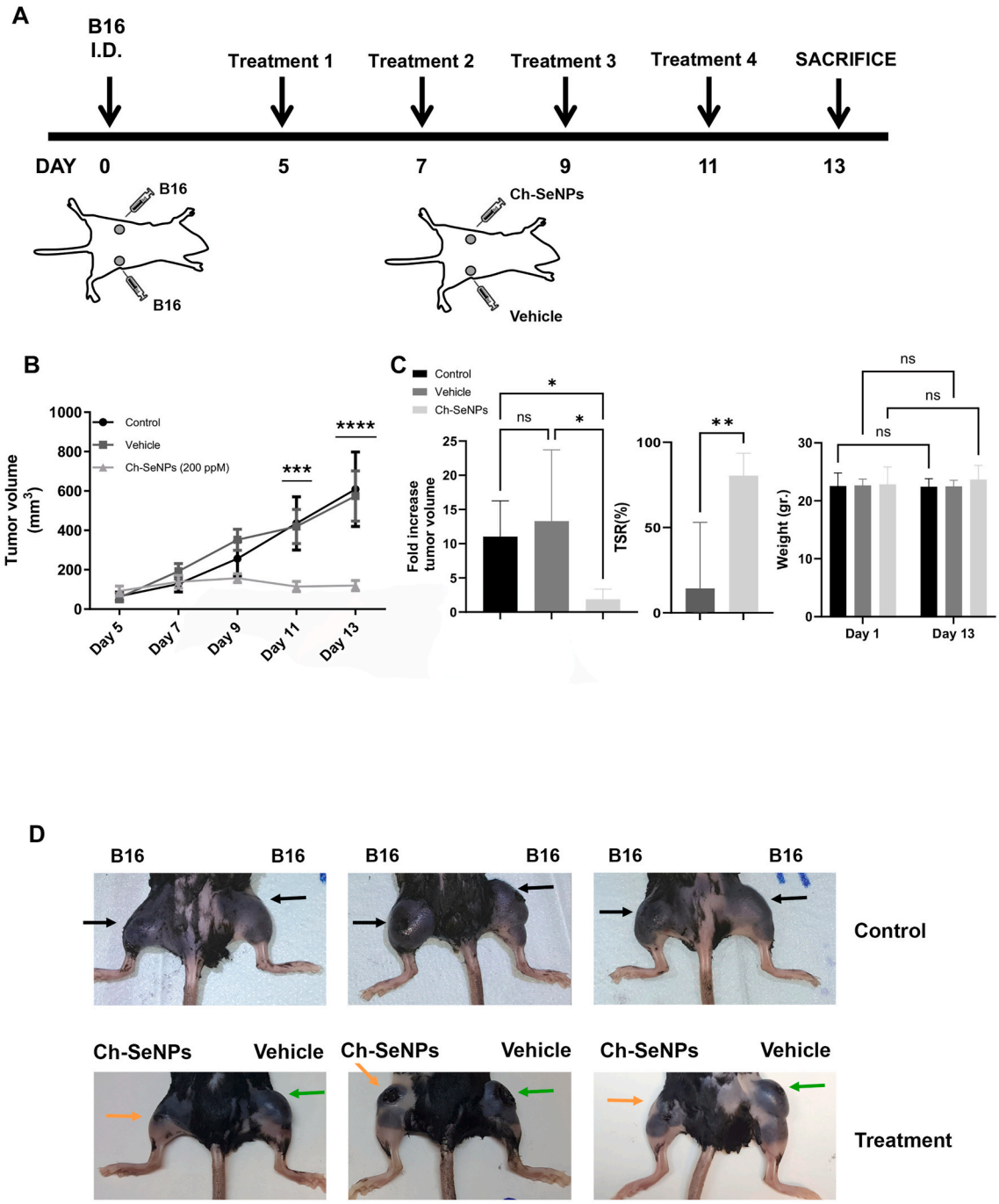

Fig. 5. In vivo experiment. (A) Timeline, (B) tumor volume, (C) tumor suppression rate analysis, (D) tumor photographs after 13 days. Data are representative of one out of two independent experiments, and error bars represent the mean ± SEM (n = 7–9 animals per group). For B and C *right*; *P* values indicate significant differences among groups for each time point, analyzed by two-way ANOVA with Tukey's post hoc test. ***P < 0.001, ****P < 0.0001. For panel C *left*; *P* values indicate significant differences among groups, analyzed by one-way ANOVA with Tukey's post hoc test. For panel C *center*; *t*-test. Statistical significance is indicated as *P < 0.05, **P < 0.01.

administration of 200 mg/L Ch-SeNPs substantially suppressed tumor growth (Fig. 5D). Furthermore, we also monitored the weight and general health parameters of mice, and we did not observe a significant body weight changes (Fig. 5C) or worsening of general health of the mice derived of the treatment with Ch-SeNPs.

4. Conclusions

In this study, we characterized chitosan-stabilized selenium nanoparticles (Ch-SeNPs), confirming their spherical morphology and homogeneous size (40–60 nm) through TEM imaging. To investigate their molecular mechanisms of action, we applied a SILAC-based quantitative proteomic approach focused on the nuclear subproteome. This strategy revealed significant alterations in 47 nuclear-enriched proteins, mainly involved in mRNA metabolism, transcription, and cell cycle regulation, thus highlighting the efficacy of the purification protocol and the nuclear impact of Ch-SeNPs. Functional analyses identified CDK1 as a central target mediating the observed S-G2/M cell cycle arrest, further validated by gene expression studies. Additionally, deregulated proteins such as PLEC, SUMO2, RSU1, and SMARCC1,

linked to tumor progression, demonstrated the broader antitumor potential of Ch-SeNPs beyond cell cycle disruption. Importantly, the in vivo evaluation of Ch-SeNPs in a murine melanoma model, significantly reduced tumor growth without adverse effects on body weight or general health, supporting their therapeutic safety and efficacy.

CRediT authorship contribution statement

Hector Estevez: Writing – original draft, Methodology, Investigation. **Estefania Garcia-Calvo:** Writing – original draft, Investigation, Formal analysis, Conceptualization. **Roberto Álvarez-Fernández Garcia:** Writing – review & editing, Investigation, Formal analysis, Conceptualization. **Raquel Sanchez-Diaz:** Methodology, Investigation. **Juan José Lazcano:** Methodology, Investigation. **Pilar Martin:** Writing – review & editing, Supervision, Formal analysis, Conceptualization. **Jose L. Luque-Garcia:** Writing – review & editing, Supervision, Resources, Project administration, Funding acquisition, Formal analysis, Conceptualization.

Declaration of competing interest

The authors declare that they have no known competing financial interests or personal relationships that could have appeared to influence the work reported in this paper.

Acknowledgements

This work was supported by Ministerio de Ciencia, Innovación y Universidades (MICIU) grants PID2020-114529RB-I00 and PID2023-150182OB-I00. PM is supported by grants from the Madrid Regional Government (S2022/BMD-7209-INTEGRAMUNE-CM), MCIN-ISCIII-Fondo de Investigación Sanitaria (PI22/01759). Hector Estevez acknowledges Ministry of Science, Innovation and Universities from the Spanish Government for a pre-doctoral fellowship (PRE2018-084196).

Data availability

Data will be made available on request.

References

[1] Y. Niu, T. He, J. Song, S. Chen, X. Liu, Z. Chen, Y. Yu, S. Chen, A new AIE multiblock poluirethane copolymer material for subcellular microfilament imaging in living cells, Chem. Commun. 54 (2017) 7541–7544, https://doi.org/10.1039/C7CC02555F.

[2] Y. Zhang, Z. Fang, D. Pan, Y. Li, J. Zhou, H. Chen, Z. Li, M. Zhu, C. Li, L. Qin, X. Ren, Q. Gong, K. Luo, Dendritic polymer-based nanomedicines remodel the tumor stroma: improve drug penetration and enhance antitumor immune response, Adv. Mater. 36 (2024) 2401304, https://doi.org/10.1002/adma.202401304.

[3] J. Liu, X. Li, Y. Li, Q. Gong, K. Luo, Metformin-based nanomedicines for reprogramming tumor immune microenvironment, Theranostics 15 (2025) 993–1016. https://www.thno.org/v15p0993.htm.

[4] Y. Niu, F.J. Stadler, T. He, X. Zhang, Y. Yu, S. Chen, Smart multifunctional polyurethane microcapsules for the quick release of anticancer drugs in BGC 823 and HeLa tumor cells, J. Mater. Chem. B 5 (2017) 9477–9481.

[5] T. Sun, Y.S. Zhang, B. Pang, D.C. Hyun, M. Yang, Y. Xia, Engineered nanoparticles for drug delivery in cancer therapy, Angew Chem. Int. Ed. Engl. 53 (2014) 12320–12364, https://doi.org/10.1002/anie.201403036.

[6] W. Tang, W. Fan, J. Lau, L. Deng, Z. Shen, X. Chen, Emerging blood-brain-barrier-crossing nanotechnology for brain cancer theranostics, Chem. Soc. Rev. 48 (2019) 2967–3014, https://doi.org/10.1039/c8cs00805a.

[7] W. Wang, J. Cai, J. Wen, X. Li, Y. Yu, L. Zhang, Q. Han, Z. Wei, Y. Ma, F. Ying, X. Xu, W. Li, Q. Yang, S. Sun, X. He, L. Cai, H. Xiao, Boosting ferroptosis via abplatin(iv) for treatment of platinum-resistant recurrent ovarian cancer, Nano Today 44 (2022) 101459.

[8] H. Estevez, E. Garcia-Calvo, J. Rivera-Torres, M. Vallet-Regi, B. Gonzalez, J. L. Luque-Garcia, Transcriptome analysis identifies novel mechanisms associated with the antitumor effect of chitosan-stabilized selenium nanoparticles, Pharmaceutics 13 (2021) 356, https://doi.org/10.3390/pharmaceutics13030356.

[9] H. Estevez, E. Garcia-Calvo, M.L. Mena, R. Alvarez-Fernandez Garcia, J.L. Luque-Garcia, Unraveling the mechanisms of Ch-SeNPs cytotoxicity against cancer cells: insights from targeted and untargeted metabolomics, Nanomaterials (Basel) 13 (2023) 2204, https://doi.org/10.3390/nano13152204.

[10] H.T. Tan, Y.H. Lee, M.C.M. Chung, Cancer proteomics. Mass Spectrom, Rev. 31 (2012) 583–605, https://doi.org/10.1002/mas.20356.

[11] E. Chen, J.R. Yates, Cancer proteomics by quantitative shotgun proteomics, Mol. Oncol. 1 (2007) 144–159, https://doi.org/10.1016/j.molonc.2007.05.001.

[12] H. Zhang, Y. Xu, P. Papanastasopoulos, J. Stebbing, G. Giamas, Broader implications of SILAC-based proteomics for dissecting signaling dynamics in cancer, Expert Rev. Proteomics 11 (2014) 713–731, https://doi.org/10.1586/14789450.2014.971115.

[13] Y. Guo, X. Deng, S. Wang, Y. Yuan, Z. Guo, H. Hao, Y. Jiao, P. Li, S. Han, SILAC proteomics based on 3D cell spheroids unveils the role of RAC2 in regulating the crosstalk between triple-negative breast cancer cells and tumor-associated macrophages, Int. J. Biol. Macromol. 254 (2023) 127639, https://doi.org/10.1016/j.ijbiomac.2023.127639.

[14] Alfonso-Garrido, J., Garcia-Calvo, E., Luque-Garcia, J.L. Sample preparation strategies for improving the identification of membrane proteins by mass spectrometry. Anal. Bioanal. Chem. 407, 4893-4905. https://doi.org/10.1007/s00216-015-8732-0.

[15] H. Estevez, J.C. Garcia-Lidon, C. Camara, J.L. Luque-Garcia, Effects of chitosan-modified selenium nanoparticles on cell proliferation, apoptosis and cell cycle pattern in HepG2 cells: Comparison with other selenospecies, Colloids Surfaces B Biointerfaces 122 (2014) 184–193, https://doi.org/10.1016/j.colsurfb.2014.06.062.

[16] Y. Bai, Y. Wang, Y. Zhou, W. Li, W. Zheng, Modification and modulation of saccharides on elemental selenium nanoparticles in liquid phase, Mater. Lett. 62 (2008) 2311–2314, https://doi.org/10.1016/j.matlet.2007.11.098.

[17] H. Liao, F. Ji, S. Ying, CDK1: beyond cell cycle regulation, Aging (Albany. NY) 9 (2017) 2465–2466, https://doi.org/10.1038/s41416-023-02468-8.

[18] T. Abbas, A. Dutta, P21 in cancer: intricate networks and multiple activities, Nat. Rev. Cancer 9 (2010) 400–414, https://doi.org/10.1038/nrc2657.

[19] S.H. Jang, A.R. Kim, N.H. Park, J.W. Park, I.S. Han, DRG2 regulates G2/M progression via the cyclin B1-Cdk1 complex, Mol. Cells 39 (2016) 699–704, https://doi.org/10.14348/molcells.2016.0149.

[20] R. Yang, C. Müller, V. Huynh, Y.K. Fung, A.S. Yee, H.P. Koeffler, Functions of cyclin A1 in the cell cycle and its interactions with transcription factor E2F-1 and the Rb family of proteins, Mol. Cell Biol. 19 (1999) 2400–2407, https://doi.org/10.1128/MCB.19.3.2400.

[21] R. Gräub, H. Lancero, A. Pedersen, M. Chu, K. Padmanabhan, X.Q. Xu, P. Spitz, R. Chalkley, A.L. Burlingame, D. Stokoe, H.S. Bernstein, Cell cycle-dependent phosphorylation of human CDC5 regulates RNA processing, Cell Cycle 7 (2008) 1795–1803, https://doi.org/10.4161/cc.7.12.6017.

[22] Y. Wang, H. Chang, D. Gao, L. Wang, N. Jiang, B. Yu, CDC5L contributes to malignant cell proliferation in human osteosarcoma via cell cycle regulation, Int. J. Clin. Exp. Pathol. 9 (2016) 10451–10457.

[23] R. Gandhi, P.J. Gillespie, T. Hirano, Human wapl is a cohesin-binding protein that promotes sister-chromatid resolution in mitotic prophase, Curr. Biol. 16 (2006) 2406–2417, https://doi.org/10.1016/j.cub.2006.10.061.

[24] F. Yi, Z. Wang, J. Liu, Y. Zhang, Z. Wang, H. Xu, X. Li, N. Bai, L. Cao, X. Song, Structural maintenance of chromosomes protein 1: role in genome stability and tumorigenesis, Int. J. Biol. Sci. 13 (2017) 1092–1099, https://doi.org/10.7150/ijbs.21206.

[25] Y.F. Zhang, R. Jiang, J.D. Li, X.Y. Zhang, P. Zhao, M. He, H.Z. Zhang, L.P. Sun, D. L. Shi, G.X. Zhang, M. Sun, SMC1A knockdown induces growth suppression of human lung adenocarcinoma cells through G1/S cell cycle phase arrest and apoptosis pathways in vitro, Oncol. Lett. 5 (2015) 749–755, https://doi.org/10.3892/ol.2013.1116.

[26] K. Oikawa, T. Ohbayashi, T. Kiyono, H. Nishi, K. Isaka, A. Umezawa, M. Kuroda, K. Mukai, Expression of a novel human gene, human wings apart-like (hWAPL), is associated with cervical carcinogenesis and tumor progression, Cancer Res. 64 (2004) 3545–3549, https://doi.org/10.1158/0008-5472.CAN-03-3822.

[27] G. Kavanaugh, R. Zhao, Y. Guo, K.N. Mohni, G. Glick, M.E. Lacy, M.S. Hutson, M. Ascano, D. Cortez, Enhancer of rudimentary homolog affects the replication stress response through regulation of RNA processing, Mol. Cell Biol. 35 (2015) 2979–2990, https://doi.org/10.1128/MCB.01276-14.

[28] K. Pang, Q. Lv, S. Ning, L. Hao, Z. Shi, G. Zang, K. Shen, X. Zhu, G. Zhu, X. Wang, C. Han, ERH is up-regulated in bladder cancer and regulates the proliferation and apoptosis of T24 bladder cancer cells, Int. J. Clin. Exp. Med. 10 (2017) 15269–15277.

[29] M.T. Weng, J. Luo, The enigmatic ERH protein: its role in cell cycle, RNA splicing and cancer, Protein Cell 4 (2013) 807–812, https://doi.org/10.1007/s13238-013-3056-3.

[30] M.K.E. Blixt, S.J. Royle, Clathrin heavy chain gene fusions expressed in human cancers: analysis of cellular functions, Traffic 12 (2011) 754–761, https://doi.org/10.1111/j.1600-0854.2011.01183.x.

[31] M.B. Olszewski, P. Chandris, B.C. Park, E. Eisenberg, L.E. Greene, Disruption of clathrin-mediated trafficking causes centrosome overduplication and senescence, Traffic 15 (2014) 60–77, https://doi.org/10.1111/tra.12132.

[32] D. Raman, J. Sai, O. Hawkins, A. Richmond, Adaptor Protein2 (AP2) orchestrates CXCR2-mediated cell migration, Traffic 15 (2015) 451–469, https://doi.org/10.1111/tra.12154.

[33] S.J. Royle, N.A. Bright, L. Lagnado, Clathrin is required for the function of the mitotic spindle, Nature 434 (2005) 1152–1157, https://doi.org/10.1038/nature03502.

[34] X. Duan, J. Zhang, S. Liu, M. Zhang, Q. Wang, J. Cheng, Methylation of nucleolar and coiled-body phosphoprotein 1 is associated with the mechanism of tumorigenesis in hepatocellular carcinoma, Oncol. Rep. 30 (2013) 2220–2228, https://doi.org/10.3892/or.2013.2676.

[35] F. Yuan, G. Li, T. Tong, Nucleolar and coiled-body phosphoprotein 1 (NOLC1) regulates the nucleolar retention of TRF2, Cell Death Discov. 3 (2017) 17043, https://doi.org/10.1038/cddiscovery.2017.43.
[36] S.J. Shin, J.A. Smith, G.A. Rezniczek, S. Pan, R. Chen, T.A. Brentnall, G. Wiche, K. A. Kelly, Unexpected gain of function for the scaffolding protein plectin due to mislocalization in pancreatic cancer, in: Proc. Natl. Acad. Sci. U.S.A., 110, 2013, pp. 19414–19419, https://doi.org/10.1073/pnas.1309720110.
[37] J.S. Seeler, A. Dejean, SUMO and the robustness of cancer, Nat. Rev. Cancer 17 (2017) 184–197, https://doi.org/10.1038/nrc.2016.143.
[38] Y. Zhou, C. Ji, M. Cao, M. Guo, W. Huang, W. Ni, L. Meng, H. Yang, J.F. Wei, Inhibitors targeting the SUMOylation pathway: a patent review 2012-2015, Int. J. Mol. Med. 41 (2018) 3–12, https://doi.org/10.3892/ijmm.2017.3231 (Review).
[39] V. Gkretsi, A. Stylianou, M. Louca, T. Stylianopoulos, Identification of Ras suppressor-1 (RSU-1) as a potential breast cancer metastasis biomarker using a three-dimensional in vitro approach, Oncotarget 8 (2017) 27364–27379, https://doi.org/10.18632/oncotarget.16062.
[40] A.B. Gurung, A. Bhattacharjee, Significance of ras signaling in cancer and strategies for its control, Oncol. Hematol. Rev. 11 (2015) 147–152, https://doi.org/10.17925/OHR.2015.11.02.147.
[41] J.P. O'Bryan, Pharmacological targeting of RAS: recent success with direct inhibitors, Pharmacol. Res. 139 (2019) 503–511, https://doi.org/10.1016/j.phrs.2018.10.021.
[42] S. Heebøll, M. Borre, P.D. Ottosen, C.L. Andersen, F. Mansilla, L. Dyrskjøt, T. F. Ørntoft, N. Tørring, SMARCC1 expression is upregulated in prostate cancer and positively correlated with tumour recurrence and dedifferentiation, Histol. Histopathol. 23 (2008) 1069–1076, https://doi.org/10.14670/HH-23.1069.
[43] K.C. Helming, X. Wang, C.W.M. Roberts, Vulnerabilities of mutant SWI/SNF complexes in cancer, Cancer Cell 26 (2014) 309–317, https://doi.org/10.1016/j.ccr.2014.07.018.
[44] M. Sancho, E. Diani, M. Beato, A. Jordan, Depletion of human histone H1 variants uncovers specific roles in gene expression and cell growth, PLoS Genet. 4 (2008) 1–17, https://doi.org/10.1371/journal.pgen.1000227.
[45] S. Koushyar, W.G. Jiang, D.A. Dart, Unveiling the potential of prohibitin in cancer, Cancer Lett. 369 (2015) 316–322, https://doi.org/10.1016/j.canlet.2015.09.012.
[46] C. Ding, X. Fan, G. Wu, Peroxiredoxin 1 – an antioxidant enzyme in cancer, J. Cell Mol. Med. 21 (2017) 193–202, https://doi.org/10.1111/jcmm.12955.
[47] S. Elgamal, I. Artsimovitch, M. Ibba, Maintenance of transcription-translation coupling by elongation factor P, mBio 7 (2016) e01373, https://doi.org/10.1128/mBio.01373-16.
[48] M. Larochelle, J.F. Lemay, F. Bachand, The THO complex cooperates with the nuclear RNA surveillance machinery to control small nucleolar RNA expression, Nucleic Acids Res. 40 (2012) 10240–10253, https://doi.org/10.1093/nar/gks838.
[49] R. Singh, Rna – protein interactions that regulate Pre-mRNA splicing, Gene Expr. 10 (2005) 79–92.
[50] T.H. Wu, L. Shi, J. Adrian, M. Shi, R.V. Nair, M.P. Snyder, P.N. Kao, NF90/ILF3 is a transcription factor that promotes proliferation over differentiation by hierarchical regulation in K562 erythroleukemia cells, PLoS One 13 (2018) e0193126, https://doi.org/10.1371/journal.pone.0193126.
[51] A.K. Gardino, M.B. Yaffe, 14-3-3 proteins as signaling integration points for cell cycle control and apoptosis, Semin. Cell Dev. Biol. 22 (2011) 688–695, https://doi.org/10.1016/j.semcdb.2011.09.008.
[52] K. Pennington, T. Chan, M. Torres, J. Andersen, The dynamic and stress-adaptive signaling hub of 14-3-3: emerging mechanisms of regulation and context-dependent protein–protein interactions, Oncogene 37 (2018) 5587–5604, https://doi.org/10.1038/s41388-018-0348-3.
[53] S. Chakraborty, A. Kumar, M.M. Faheem, A. Katoch, A. Kumar, V.L. Jamwal, D. Nayak, A. Golani, R.U. Rasool, S.M. Ahmad, J. Jose, R. Kumar, S.G. Gandhi, L. Dinesh Kumar, A. Goswami, Vimentin activation in early apoptotic cancer cells errands survival pathways during DNA damage inducer CPT treatment in colon carcinoma model, Cell Death Dis. 10 (2019) 46, https://doi.org/10.1038/s41419-019-1690-2.
[54] M. Cerezo, S. Rocchi, New anti-cancer molecules targeting HSPA5/BIP to induce endoplasmic reticulum stress, autophagy and apoptosis, Autophagy 13 (2017) 216–217, https://doi.org/10.1080/15548627.2016.1246107.
[55] K.F. Lee, M.M. Tsai, C.Y. Tsai, C.G. Huang, Y.H. Ou, C.C. Hsieh, H.L. Hsieh, C. S. Wang, K.H. Lin, DEK is a potential biomarker associated with malignant phenotype in gastric cancer tissues and plasma, Int. J. Mol. Sci. 20 (2019) 5689, https://doi.org/10.3390/ijms20225689.
[56] X. Liu, K.M. Chu, α-Actinin-4 promotes metastasis in gastric cancer, Lab. Invest. 97 (2017) 1084–1094, https://doi.org/10.1038/labinvest.2017.28.
[57] Z. Yang, L. Zhuang, P. Szatmary, L. Wen, H. Sun, Y. Lu, Q. Xu, X. Chen, Upregulation of heat shock proteins (HSPA12A, HSP90B1, HSPA4, HSPA5 and HSPA6) in tumour tissues is associated with poor outcomes from HBV-related early-stage hepatocellular carcinoma, Int. J. Med. Sci. 12 (2015) 256–263, https://doi.org/10.7150/ijms.10735.
[58] W.W. Overwijk, N.P. Restifo, B16 as a mouse model for human melanoma, Curr. Protoc. Immunol. Chapter 20 (2001), https://doi.org/10.1002/0471142735.im2001s39. Unit 20.1.
[59] I. Lopez Heras, R. Sanchez-Diaz, D.S. Anunciaçao, Y. Madrid, J.L. Luque-García, C. Camara, Effect of chitosan-stabilized selenium nanoparticles on cell cycle arrest and invasiveness in Hepatocarcinoma cells revealed by quantitative proteomics, J. Nanomed. Nanotechnol. 5 (2014) 1, https://doi.org/10.4172/2157-7439.1000226.